Relativistic calculations of the hyperfine interactions in the excited $7\,^2P_{3/2}$ and $7\,^2P_{1/2}$ states of the Ra^+ ion

Xing Yuan, R. W. Dougherty,* and T. P. Das
Department of Physics, State University of New York at Albany, Albany, New York 12222

J. Andriessen
Technische Natuurkunde, Technische Universiteit Delft, 2628 CJ Delft, The Netherlands
(Received 16 June 1995)

The relativistic linked-cluster many-body perturbation theory (RLCMBPT) has been used to investigate the hyperfine properties in the excited $7\,^2P_{3/2}$ and $7\,^2P_{1/2}$ states of $^{221}Ra^+$ ions. Our calculations of the hyperfine constants yield -22.4 ± 0.3 MHz for the $7\,^2P_{3/2}$ state and -265.3 ± 4.0 MHz for the $7\,^2P_{1/2}$ state, in excellent agreement with the experimentally obtained values of -22.4 ± 0.9 and -266.3 ± 1.5 MHz, respectively. The results obtained in this work are compared with those by other theoretical methods and an attempt is made to understand the relationship between the different methods, particularly that between the RLCMBPT procedure adopted in this work and the many-body multiconfigurational Dirac-Fock procedures.

PACS number(s): 31.30.Gs, 31.30.Jv, 31.25.−v, 32.10.−f

I. INTRODUCTION

The relativistic linked-cluster many-body perturbation theory (RLCMBPT) [1] has been successfully applied to obtain theoretical results for the hyperfine properties of the ground states of many atomic and ionic systems involving single s valence electrons, that are found to be in good agreement with the results of experimental measurements. This has been demonstrated consistently [2] in a series of RLCMBPT calculations involving the hyperfine interactions for all the systems in the alkali-metal atom series [3], the isoelectronic positive alkaline-earth-metal ion series [2,4], the noble-metal atom series [5] and the positive group-IIB ions [6] isoelectronic with noble-metal atoms. These investigations have provided [1–6] a quantitative understanding of the origin of the hyperfine interaction as a whole in a fully relativistic framework for these various systems. Additionally, through the use of the ability of RLCMBPT to provide contributions from individual mechanisms involved in the hyperfine interactions, detailed physical insights have been obtained regarding the factors contributing to the trends in the contributions from these mechanisms, namely, the valence contribution, the exchange core polarization (ECP), and the many-body correlation effect for the four series of systems with similar electronic structures investigated. The present work regarding the hyperfine structures for the excited $7\,^2P_{3/2}$ and $7\,^2P_{1/2}$ states of the Ra^+ ion is the natural extension of our previous RLCMBPT investigations for $7\,^2S_{1/2}$ ground-state systems, the motivations being that first of all, the Ra^+ ion is a relatively heavy system in which relativistic effects would play an important role for hyperfine interactions and the experimental values are readily available for the excited P states [7] for comparison with theory. Secondly, as illustrated in the nonrelativistic evaluations of the hyperfine interactions in atomic systems [8], since in the language of nonrelativistic theory, the excited P states will have orbital and dipolar contributions in addition to the contact interaction (which is the sole contributor in the case of ground S states), a successful application of the RLCMBPT theory under this more complex situation would provide additional confidence regarding its accuracy for nonspherical systems. Lastly, there have been some other theoretical calculations on the hyperfine constants of excited $7\,^2P_{3/2}$ and $7\,^2P_{1/2}$ states for the Ra^+ ion, involving procedures such as many-body multiconfigurational Dirac-Fock (MB-MCDF) theory [9], the differential equation (DE) technique [10], and a procedure [11] that combines the many-body perturbation method with the differential equation approach. We believe a comparison of the results of our present calculation using RLCMBPT with those obtained through other theoretical methods would provide a better understanding of the factors contributing to hyperfine interactions as well as valuable insights into the physical reasoning in these different approaches.

In Sec. II a brief summary will be presented of some theoretical aspects of the RLCMBPT procedure adopted in our calculations. Section III presents our results, their comparison with experiment, and discussions. A comparison with the results of other theoretical calculations will be given in Sec. IV. Section V will present some concluding remarks and suggestions for future investigations.

II. PROCEDURE

The major aspects of the relativistic linked-cluster many-body perturbation theory pertinent to the hyperfine interactions in atomic systems have been discussed in detail in the literature [1,12]. Only a brief summary of the theory will be given here both for the sake of completeness and to be of help in discussions to be presented in later sections.

To obtain the electronic properties of an atomic system, one needs a complete knowledge of the electronic wave function Ψ_0 of the system. Relativistically, this can be

*Present address: Condensed Matter Radiation Division, Naval Research Laboratory, Washington, DC 20375.

achieved by solving the Dirac equation [13–16]

$$H\Psi_0 = E\Psi_0 \tag{1}$$

in which H is the relativistic Hamiltonian that describes the system, and E and Ψ_0 are, respectively, the total energy and the many-electron wave function of the system involved. The Hamiltonian H for an atomic system with nuclear charge ζ and N electrons is given by

$$H = \sum_{i=1}^{N} (c\boldsymbol{\alpha}_i \cdot \mathbf{p}_i + \beta_i mc^2) - \sum_{i=1}^{N} \frac{\zeta e^2}{r_i} + \sum_{i>j} \frac{e^2}{r_{ij}}, \tag{2}$$

where e and m represent electronic charge and mass, $\boldsymbol{\alpha}_i$ and β_i are the Dirac matrices for the ith electron, with $\mathbf{r}_i$ being its position vector with respect to nucleus and $\mathbf{p}_i$ its momentum vector, and r_{ij} the distance between the ith and jth electrons. The influence of Breit interactions [16,17] between the electrons is expected to have very little effect on the hyperfine interactions in systems involving a single valence electron.

The exact solution of the wave function Ψ_0 in Eq. (1) cannot be obtained because of the electron-electron interactions in the system as represented by the last term of the Hamiltonian H. With the RLCMBPT procedure, one uses a perturbation approach to solve this problem by dividing H into a zeroth-order approximation part H_0, the eigenfunction of which can be solved precisely, and a perturbation Hamiltonian H', namely,

$$H = H_0 + H'. \tag{3}$$

The zeroth-order approximation H_0 is chosen to be

$$H_0 = \sum_{i=1}^{N} (c\boldsymbol{\alpha}_i \cdot \mathbf{p}_i + \beta_i mc^2) - \sum_i \frac{\zeta e^2}{r_i} + \sum_i V(r_i) = \sum_i h_0 \tag{4}$$

in which $V(r_i)$ is a one-electron potential, for which the eigenfunction Φ_0 is given by

$$H_0\Phi_0 = E_0\Phi_0 \tag{5}$$

and can be solved precisely, since H_0 does not explicitly contain any electron-electron interactions, the influence of the last term in Eq. (2) having been incorporated approximately in $V(r_i)$ in Eq. (4). The many-electron function Ψ_0 is the determinantal function based on the occupied one-electron eigenstates φ_i of h_0 in Eq. (4) given by

$$h_0 = (c\boldsymbol{\alpha}\cdot\mathbf{p} + \beta mc^2) - \frac{\zeta e^2}{r} + V(r). \tag{6}$$

It has been the usual practice in the literature [1,18] to choose for $V(r)$ a V^{N-1} potential defined by the relation

$$\langle a|V^{N-1}|b\rangle = \sum_{n=1}^{N-1} \left(\left\langle an\left|\frac{e^2}{r_{12}}\right|bn\right\rangle - \left\langle an\left|\frac{e^2}{r_{12}}\right|nb\right\rangle \right), \tag{7}$$

with n referring to the occupied states 1 to N. The occupied state N left out of the summation is usually the valence state, which for the excited Ra^+ $^2P_{1/2}$ and $^2P_{3/2}$ states studied in this paper are the $7p_{1/2}$ and $7p_{3/2}$ states, respectively. The V^{N-1} choice for $V(r)$ provides [1,18,19] both bound and continuum excited states, allowing for better convergence in perturbation theory than the V^N choice where the summation over n in Eq. (7) is taken over all the occupied states, the excited states for the latter choice having only continuum character for neutral atoms. For positive ions one can have a few bound excited states. It has been shown in the literature [20] that a number of the diagrams for the V^{N-1} potential can be regrouped into a smaller number of diagrams if one uses Dirac-Hartree-Fock (V^N potential) wave functions for the occupied states and excited states in the V^{N-1} potential. As in our earlier RLCMBPT investigations on the ground state of Ra^+ and related systems [2–6], we shall use this prescription in the present work.

Since Ra^+ is a rather heavy system, it is necessary [21] to use a nucleus with a distributed charge rather than a point nucleus approximation. As in earlier investigations, we have employed a uniform distribution [22] over a sphere of radius $1.2A^{1/3}$ fm where A is the mass number of the Ra nucleus, 221, used in our present investigations.

As defined in Eq. (3), the perturbation Hamiltonian H' is the difference between the true Hamiltonian H of the system and the zeroth-order approximation (unperturbed) Hamiltonian H_0, namely,

$$H' = H - H_0 = \sum_{i>j} \frac{e^2}{r_{ij}} - \sum_i V_i^{N-1}. \tag{8}$$

The solution of the Dirac equation (1), the exact many-electron wave function Ψ_0 of the system, can now be expressed by the linked-cluster expansion [23] in terms of the unperturbed wave function Φ_0, namely,

$$\Psi_0 = \sum_{n=0}^{\infty} \left(\frac{H'}{E_0 - H_0}\right)^n \Phi_0. \tag{9}$$

Having obtained Ψ_0, the hyperfine properties of the atomic system can be calculated as the expectation value of the hyperfine interaction Hamiltonian $H'_{\rm hyp}$ over Ψ_0. For the relativistic treatment of magnetic hyperfine properties, $H'_{\rm hyp}$ is given by

$$H'_{\rm hyp} = ec \sum_i \boldsymbol{\alpha}_i \frac{\boldsymbol{\mu}_I \times \mathbf{r}_i}{r_i^3} \tag{10}$$

in which $\boldsymbol{\mu}_I$ is the nuclear magnetic moment vector of the system. The expectation value

$$\langle \Psi_0 | H'_{\rm hyp} | \Psi_0 \rangle = \sum_{m,n}^{(L)} \left\langle \Phi_0 \left| \left(\frac{H'}{E_0 - H_0}\right)^m H'_{\rm hyp} \left(\frac{H'}{E_0 - H_0}\right)^n \right| \Phi_0 \right\rangle \tag{11}$$

is related [1] to the hyperfine constant A_J in the form of

$$A_J = \frac{1}{IJ} \langle \Psi_0 | H'_{\rm hyp} | \Psi_0 \rangle \tag{12}$$

with I referring to the spin of the nucleus and J the magnitude of the total electronic angular momentum corresponding to Ψ_0.

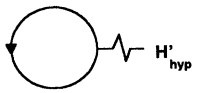

FIG. 1. (0,0) diagram. Direct valence contribution to the hyperfine constant.

Each term in the expansion (11) corresponding to specific m and n values is referred to as a (m,n) term and can be expressed graphically in terms of diagrams. The rules for drawing these diagrams and the corresponding mathematical expressions for their evaluation, involving matrix elements of the perturbation Hamiltonian H' and the hyperfine operator $H'_{\rm hyp}$ over one-electron occupied and excited states and corresponding energy denominators, have been discussed in detail in earlier literature [19]. Also, the value $m+n$ for each term in the summation in Eq. (11) represents the order of the perturbation in H'. As can be seen from Eq. (11), the (m,n) and (n,m) terms for a specific set of m and n values are mathematically equivalent and therefore one needs only to evaluate one of them and multiply by a factor of 2 to obtain the sum of the two terms.

The major contributors to the magnetic hyperfine constants in atomic systems are characterized in different categories [1,19] according to the physical mechanisms for their contribution to the hyperfine interaction. The zeroth-order perturbation (0,0) term, referred to as a direct or valence contribution, is shown diagrammatically in Fig. 1. The first-order contributions represented by (0,1) or (1,0) terms are called the ECP and phase-space contributions, some typical diagrams corresponding to these different effects being represented by Fig. 2. The second-order perturbation (1,1) and (0,2) or (2,0) terms are referred to as exclusion principle violating (EPV), various first-order consistency, and second-order many-body correlation effects and are shown in Figs. 3, 4, and 5. For perturbation terms higher than second order $(m+n>2)$, most of their contributions to the hyperfine interaction are found to be negligible in many of the cases [2–6] we have studied. A few of them do make nonvanishing contributions and diagrams corresponding to them are shown in Fig. 6.

III. RESULTS

The results of our calculations of the hyperfine constants of $^{221}Ra^+$ for the excited $7\ ^2P_{3/2}$ and $7\ ^2P_{1/2}$ are presented in Table I. Also included in this table are the experimental values of the hyperfine constants for these two states. The nuclear magnetic moment of the $^{221}Ra^+$ isotope used in our investigations is -0.179 nuclear magneton [24] and the nuclear spin is $\frac{5}{2}$.

In order to better understand the physical aspects of the theoretical values obtained through this RLCMBPT investigation, we will give detailed breakdowns in our results according to the physical mechanisms prescribed by the RLCMBPT procedure.

A. Direct (or valence) contribution

This is the direct contribution to the hyperfine constants from the valence electron $7p_{3/2}$ and $7p_{1/2}$ for the $7\ ^2P_{3/2}$ and $7\ ^2P_{1/2}$ excited states of Ra^+, respectively, as represented by the (0,0) diagram in Fig. 1. The calculated results for this effect are presented in the first row of Table I. Clearly they are the leading contributors to the hyperfine interactions.

B. Exchange core polarization effect

The contributions from the ECP effect are given in the second row of Table I and the corresponding diagram for this effect is shown in Fig. 2(a). This effect arises from the fact [19] that the valence electron can have exchange interaction only with core electrons with the same spin as the valence itself. This exchange interaction will lead to a difference between the potential experienced by core electrons with the same and opposite spins with respect to the valence electron, thus leading to a perturbation potential that can contribute to the hyperfine interaction. The contributions to the ECP effect from individual core shells for each of the excited states $7\ ^2P_{3/2}$ and $7\ ^2P_{1/2}$ are given in Table II. The major con-

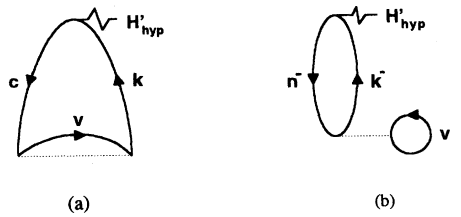

FIG. 2. Typical (0,1) diagrams. Diagrams representing (a) exchange core polarization (ECP), and (b) phase-space contributions to the hyperfine constant.

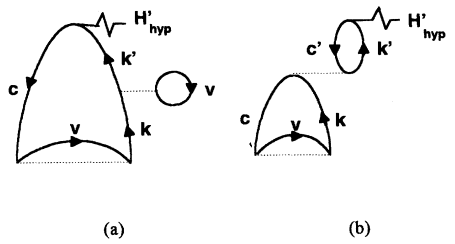

FIG. 3. Typical (0,2) diagrams. Diagrams representing (a) exclusion principle violation (EPV), and (b) consistency contributions to the hyperfine constant.

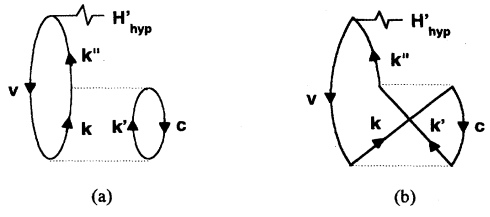

FIG. 4. Typical (0,2) diagrams. Diagrams representing second-order (a) direct, and (b) exchange, correlation contributions to the hyperfine constant.

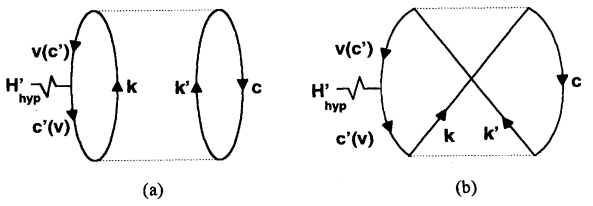

FIG. 5. Typical (1,1) diagrams. Diagrams representing second-order (a) direct, and (b) exchange, correlation contributions to the hyperfine constant.

tributors are the $s_{1/2}$ core shells in both cases, and the $p_{3/2}$ core shells for the $7\ ^2P_{3/2}$ and $p_{1/2}$ core shell for the $7\ ^2P_{1/2}$ case. The former could be easily understood because the s wave function has the strongest interaction with the nucleus thus leading to a large contribution to the ECP effect. For the $7\ ^2P_{3/2}$ excited state, the $p_{3/2}$ core electrons have the strongest exchange interactions with the $7p_{3/2}$ valence electron and therefore make an important contribution to the ECP result. The same reasoning can explain the substantial ECP contribution from the $p_{1/2}$ core electrons in the $7\ ^2P_{1/2}$ case.

C. Phase-space contribution

The phase-space contribution [19] is given in the third line of Table I, the corresponding diagram being shown in Fig. 2(b). The phase-space effect is associated with the fact that the valence state with down spin is empty and available for excitation from down-spin core states while the up-spin valence state is occupied (by the valence electron) and therefore not available for excitation for the up-spin core electrons, thus leading to a difference in contributions from core electrons with opposite spin. This effect is substantially smaller than the ECP effect because of the larger amount of available phase space (all the bound and continuum excited states) for excitations in the latter case.

D. Exclusion principle violating effect

Line 4 of Table I gives the calculated results for this contribution and the corresponding diagram is shown in Fig. 3(a). As discussed in Sec. II, a V^{N-1} potential is chosen instead of the Hartree-Fock V^N potential when generating the excited states of the unperturbed system. This modification will cause changes in the potential experienced by the electrons in the core ground states as compared to the Hartree-Fock potential. The EPV diagram [19] corrects for the effect of this potential change.

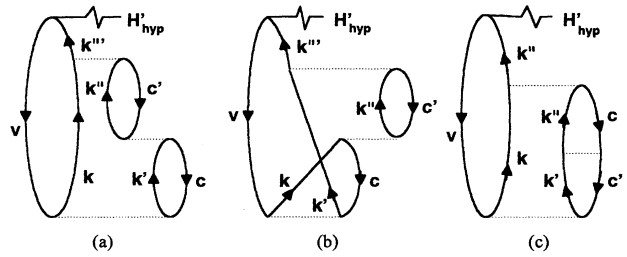

FIG. 6. Major third-order correlation diagrams. (0,3) diagrams representing (a) direct, and (b) exchange, correlation contributions to the hyperfine constant.

TABLE I. Results of hyperfine constant calculations in $^{221}Ra^+$ for the $7\ ^2P_{3/2}$ and $7\ ^2P_{1/2}$ excited states (in MHz).

Mechanism	$7\ ^2P_{3/2}$	$7\ ^2P_{1/2}$
Valence	−13.7	−181.4
ECP	−6.0	−50.3
Phase space	0.3	3.3
EPV	0.6	4.5
Consistency	−0.5	−7.9
net ECP	−5.6	−50.4
Correlation		
(0,2) correlation	−3.4	−35.8
(1,1) correlation	0.3	−1.1
third-order correlation	0.0	3.4
Correlation total	−3.1	−33.5
Total	−22.4±0.3	−265.3±4.0
Experiment [a]	−22.4±0.9	−266.3±1.5

[a]Reference [7].

E. Consistency effect

The consistency effect represented by the diagram in Fig. 3(b) illustrates the influence of the self-consistent interaction between electrons. When a core state is perturbed through its exchange with the valence state (leading to the ECP effect), its interaction with electrons in other states can cause changes in these latter states and consequently lead to additional contributions [19,25] to the hyperfine field. Our calculated results for this particular effect are listed in the fifth row of Table I.

In the RLCMBPT theory, the last four effects, the ECP, phase-space, EPV, and consistency effects represent the contribution to the hyperfine properties from one-electron interactions. They are usually grouped together and their totality is referred to as the "net ECP" effect listed in the sixth row of Table I.

F. Many-body correlation effects

The many-body correlation contributions [1,19,25] to the hyperfine constants of Ra^+ in excited $7\ ^2P_{3/2}$ and $7\ ^2P_{1/2}$ states are given in the seventh and eighth lines in Table I. Among them, the second-order effects described by diagrams in Figs. 4 and 5, representing direct and exchange diagrams,

TABLE II. Breakdown of contribution to the ECP effect from different core shells in the $7\ ^2P_{3/2}$ and $7\ ^2P_{1/2}$ excited state of Ra^+ system (in MHz).

Core shells	$7\ ^2P_{3/2}$	$7\ ^2P_{1/2}$
$s_{1/2}$	−3.5	−13.3
$p_{1/2}$	−0.2	−32.3
$p_{3/2}$	−2.5	−3.0
$d_{3/2}$	0.2	−2.6
$d_{5/2}$	+0.0	0.9
Total	−6.0	−50.3

TABLE III. Hyperfine constants (in MHz) for the excited 7 $^2P_{3/2}$ and 7 $^2P_{1/2}$ states of the $^{221}Ra^+$ ion calculated by different theoretical methods.

	7 $^2P_{3/2}$				7 $^2P_{1/2}$			
Procedure	Valence	Net ECP	Correlation	Total	Valence	Net ECP	Correlation	Total
RLCMBPT	−13.7	−5.6	−3.1	−22.4	−181.4	−50.4	−33.5	−265.3
MB-MCDF [a]	−13.9	−7.9	−0.7	−22.5	−182.6	−35.5	−39.2	−257.3
DE [b]	−13.3	−8.9			−176.6	−34.1		
MBPT-DE [c]	−13.3	−8.4	−0.6	−22.3	−173.2	−31.9	−56.7	−261.8
Experiment [d]				−22.4				−266.3

[a]Reference [9].
[b]Reference [10].
[c]Reference [11].
[d]Reference [7].

make the dominant contribution. The correlation effect occurs for the first time in second order when one considers the electron-electron interaction in Eq. (11) corresponding to the $m+n=2$ terms in the perturbation expansion. Of the two types of second-order correlation effect, the contribution from (0,2) diagrams in Fig. 4 dominate over those from the (1,1) diagrams represented by Fig. 5, as has also been found in systems [2–6] with a single s valence electron. The ninth line of Table I lists our estimates of the third-order correlation contribution. They are considered as estimates because we have analyzed only a few third-order diagrams, some typical ones being shown in Fig. 6. These diagrams are chosen on the basis that they are related to the direct and exchange (0,2) diagrams (Figs. 4 and 5) which make dominant contributions to the correlation effect in the second order. The net correlation effect is listed in the tenth line.

The net calculated values of the hyperfine constants and the confidence limits placed on these results are listed in the 11th line of Table I. The latter are obtained through the consideration [2–6,19] of higher-order diagrams that are not included in our evaluation as well as the computational accuracy of the calculation.

Finally, the results of the experimental measurements [7] of the hyperfine constant in the excited 7 $^2P_{3/2}$ and 7 $^2P_{1/2}$ states of $^{221}Ra^+$ are given in the last row of Table I. They are seen to be in excellent agreement with our theoretical values calculated through the application of the RLCMBPT procedure.

IV. DISCUSSION

As mentioned in Sec. I, there are a number of other theoretical calculations of the hyperfine constants in the excited 7 $^2P_{3/2}$ and 7 $^2P_{1/2}$ states of the $^{221}Ra^+$ ion in the literature by different procedures than the RLCMBPT method adopted here. These other investigations involve the many-body multiconfigurational Dirac-Fock method [9], the differential equation method [10], and a process [11] that combines the many-body perturbation approach with the DE method. In this section, we will discuss the physical features of the approaches involved in the earlier calculations and attempt to understand the nature of their results as compared to those obtained by the present investigation involving the RLCMBPT procedure. We have listed results from the other investigations as well as ours in Table III, along with the breakdown of the net hyperfine constants according to the direct, net ECP, and many-body correlation contributions.

The first row of Table III lists the result of the present work for the hyperfine constants in the excited 7 $^2P_{3/2}$ and 7 $^2P_{1/2}$ states of the $^{221}Ra^+$ ion, both the total values as well as the separate contributions from three types of physical effects. The second line of Table III represents the results obtained by the MB-MCDF method. We shall first compare the results by these two methods, because they are closely related from a physical point of view although they involve different mathematical and computational procedures.

The MB-MCDF approach [9] is based on the principles of the RLCMBPT procedure as well as the MCDF method [26]. The major aspects of the RLCMBPT procedure have been summarized in Sec. II and will not be repeated here. The detailed description of the MCDF approach is available in the literature [9,26] and we will only give some of its major points here to facilitate our discussion.

For the MCDF approach, in order to solve the many-electron Dirac equation, Eq. (1), the total wave function of the atomic system Ψ_0 is expressed in terms of a series of determinantal wave functions Φ_j corresponding to different configurations involving different sets of N occupied one-electron states φ_j, N being the total number of electrons in the atom. Thus,

$$\Psi_0(r_1,\ldots,r_n;J,M)=\sum_{j=1}^{m} C_j\Phi_j(\varphi_1,\varphi_2,\ldots,\varphi_N;J,M), \tag{13}$$

where m is the number of configurations employed for the variational treatment of the many-electron wave function Ψ. The one-electron wave functions φ_j are coupled to form the individual determinants Φ_j, which in turn are combined together to form Ψ_0, all of the determinants Φ_j and Ψ_0 with total angular momenta J and M. The following functional is then optimized with respect to C_j and φ_j, namely,

$$E(\Psi_0)=\frac{\langle\Psi_0|H|\Psi_0\rangle}{\langle\Psi_0|\Psi_0\rangle} \tag{14}$$

in which H is the Hamiltonian of the system represented by Eq. (1.5) and φ_i can be expressed in terms of the relativistic form [16]

$$\varphi_i(r)=\frac{1}{r}\begin{pmatrix} p_i(r)\chi_{\kappa m}(\theta,\phi) \\ -iq_i(r)\chi_{-\kappa m}(\theta,\phi)\end{pmatrix}, \tag{15}$$

where $p_i(r)$ and $q_i(r)$ are the radial parts of the large and small components of the wave function φ_i, and $\chi_{\pm\kappa m}(\theta,\phi)$ are the two-dimensional spinors describing the angular factors (for both orbit and spin parts) of the wave function.

Using standard variational techniques, the above optimization leads to a set of equations for the expansion coefficients C_j as well as differential equations for the radial wave functions $p_i(r)$ and $q_i(r)$. These equations can be solved using well established numerical procedures and the computer programs [27] developed to obtain the exact total wave function Ψ_0 and subsequently the total energy E of the system.

With the MCDF method, when calculating properties of the atomic system, in this case, the hyperfine constant characterized by its Hamiltonian $H'_{\rm hyp}$ of Eq. (10), one needs [9] to get a new total wave function Ψ and the total energy E_A of the system that corresponds to the addition of this $H'_{\rm hyp}$ to the Hamiltonian in Eq. (2). The total Hamiltonian of the system, including the hyperfine interaction effect, would then be given by

$$H_A=\sum_{i=1}^{N}(c\boldsymbol{\alpha}_i\cdot\mathbf{p}_i+\beta_i mc^2)-\sum_{i=1}^{N}\frac{\zeta e^2}{r_i}+\sum_{i>j}\frac{e^2}{r_{ij}}$$
$$+ec\sum_i\boldsymbol{\alpha}_i\frac{\boldsymbol{\mu}_I\times\mathbf{r}_i}{r_i^3}. \tag{16}$$

The new total energy of the system can be expressed as

$$E_A(\Psi)=\frac{\langle\Psi|H_A|\Psi\rangle}{\langle\Psi|\Psi\rangle} \tag{17}$$

and the trial function Ψ for the eigenfunction of H_A by the equation

$$\Psi(r_1,\ldots,r_N;J,M)$$
$$=\sum_{j_A=1}^{m}C_{j_A}\Phi_{j_A}(\varphi_1,\ldots,\varphi_i,\ldots,\varphi_N;J,M). \tag{18}$$

The total energy optimization can be carried out using the same procedure just mentioned for Eq. (13) through Eq. (15), however, now one uses the new Hamiltonian H_A and the total wave function Ψ in Eq. (18) instead of H and Ψ_0[Eqs. (2) and Eq. (13)]. This produces a fresh set of equations for the expansion coefficients C_{j_A} and new differential equations for the components of the wave functions in which the effect of the hyperfine interaction has been included. By solving these equations, one can obtain the eigenfunction and total energy E_A corresponding to the Hamiltonian H_A, which represents the atomic system including the effect of hyperfine interaction. The energy difference between Eq. (17) and Eq. (14) would be the hyperfine interaction in the total energy term and can be converted, using a formula similar to Eq. (12), to the hyperfine constant in MHz, which can be compared with the results of experimental measurements.

Because of the relatively small magnitude of the hyperfine interaction, it is essential to have very accurate information about the wave function in order to calculate hyperfine properties in atomic systems. For the MCDF method, this is necessary because one calculates the hyperfine interaction energy from the difference between the total energy E_0 and E_A corresponding to the Hamiltonian H_0 and H_A. One thus requires very accurate calculations of the corresponding eigenvalues E and E_A so that the errors in these terms do not overshadow the small hyperfine energy. This then requires incorporation of inordinately large numbers of configurations in Eqs. (13) and (18) so that both the hyperfine-independent and hyperfine-dependent contributions to the total energies are obtained very accurately. The use of such large numbers of configurations entails the solutions of correspondingly large numbers of differential Dirac-Hartree-Fock type equations for φ_i, which can be very time consuming. The MB-MCDF theory [9] overcomes this problem by incorporating the perturbation concept and the diagrammatic technique of the RLCMBPT approach into the MCDF method.

For the hyperfine properties in atomic systems, it has been demonstrated in the earlier literature [9] that a link can be established between the perturbation expansion of Eq. (9) for the first- and second-order ($n\leqslant 2$) terms in the RLCMBPT procedure and the configuration expansion in Eq. (18) in the MCDF method. For the single valence electron contribution to the hyperfine constant, the configuration expansion of Eq. (18) involves only the ground-state determinantal wave function Φ_1. The energy difference between Eqs. (14) and (17) is expected to be the same as the (0,0) term from the valence electron in the hyperfine interaction perturbation expansion Eq. (9) of the RLCMBPT method shown by the diagram in Fig. 1. Instead of taking this energy difference, one calculates just the expectation value of the hyperfine interaction Hamiltonian with the Hartree-Fock wave functions for Ra^+ just as in the RLCMBPT procedure. The closeness of the valence electron contribution from our RLCMBPT calculations and the earlier MB-MCDF results [9] in Table III suggests that both calculations have the correct result at the (0,0) level.

Considering the ECP and phase-space diagrams represented at the (0,1) level by Figs. 2(a) and 2(b), one can use, for instance, excitations of the form $1s$-$6s\rightarrow ks$ where the core s electrons $1s$ through $6s$ are excited to higher states ks. Instead of taking a set of higher ks in Eq. (13) for excitations of each of the core states $1s$-$6s$, MB-MCDF uses a general ks and determines the excited-state function φ_{ks} by solving the Dirac equation for it, using the minimization process in Eq. (14). One can similarly consider excitations of the $2p$-$6p$ core states and $3d$-$5d$ core states to kp and kd, respectively, and using the combined functions in Eq. (13) to get the appropriate contributions to the ECP and phase-space diagrams Figs. 2(a) and 2(b) from diagonal excitations of the core states, that is states of same $l(\kappa)$. However, from our RLCMBPT work [8] one finds, as expected from the influence of the $1/r_{12}$ electron-electron interaction vertex in Figs. 2(a) and 2(b), that there can be significant contributions from nondiagonal or angular excitation of the type $6s\rightarrow kd$, $6p\rightarrow kf$, and $5d\rightarrow ks,kg$ which can contribute to the "dipo-

lar" components of the hyperfine interaction vertex in the nonrelativistic approximation. There could of course also be $p \rightarrow p$ and $d \rightarrow d$ excitations due to the dipolar components of the hyperfine interaction. These interactions have not been included in the MB-MCDF work [9] on the present systems. Correspondingly, the consistency effects from the angular excitations are also not included in the latter work while they are included in the present work. The above considerations may account for part of the difference in the net ECP contributions between the two calculations, our analysis of the corresponding RLCMBPT contributions suggesting, however, that this error could at most account for about 15% of the difference between the results of these two procedures.

For the correlation diagrams like the leading ones of the (0,2) type diagrams shown in Figs. 4(a) and 4(b), one has to consider pair correlation effects involving simultaneous excitations associated with two orbitals, for instance, $(7p,6p) \rightarrow (kp,k'p)$ and $(7p,6p) \rightarrow (nf,nf')$ at the first $1/r_{12}$ vertex and corresponding two-electron excitations at the second $1/r_{12}$ vertex which returns the core electron $6p$ to its original state and leaves the valence $7p_{1/2}$ or $7p_{3/2}$ electron in an excited state. In the MB-MCDF calculations [9], excitations in Figs. 4(a) and 4(b) of the type $7p \rightarrow nf$ after the second pair excitation are not included. This then leads to the omission of some of the (0,2) correlation diagrams, just as was the case for the ECP diagrams. In addition, the (0,2) correlation diagrams corresponding to excitations of the d core states, especially the $5d$ core electron which makes a large contribution as compared to $3d$ and $4d$ core electrons, have not been included in the MB-MCDF procedure. For the (1,1) correlation diagrams in Figs. 5(a) and 5(b), a parallel procedure involving first pair $1/r_{12}$ excitation and then a single excitation due to the hyperfine vertex, has been adopted in the MB-MCDF procedure. This contribution, however, has been found from our RLCMBPT calculations to be rather small compared to that from the (0,2) diagrams. A consideration of the angular excitation contributions from the (0,2) diagrams in our RLCMBPT work suggests they cannot account for more than 10% of the difference in the two results in Table III. However, the neglect of the pair excitations involving the d core electrons in the MB-MCDF method contributes about 40% of the difference in the correlation contributions. That still leaves about half of the difference to be explained.

Therefore it seems that while there is quite good agreement between the net contributions to the hyperfine constants for the $^2P_{3/2}$ and $^2P_{1/2}$ states of Ra^+ by the RLCMBPT and MB-MCDF procedures, there are significant differences between the net ECP and correlation contributions which tend to nearly cancel each other out for the $^2P_{3/2}$ state and partially for the $^2P_{1/2}$ state. Studies for more systems by the two procedures are needed in order to explain this situation, with the MB-MCDF [9] calculations being carried out in a way that will provide a more detailed correspondence between individual diagrams and excitations of one electron states for ECP and correlation processes with the RLCMBPT procedure.

The third line of Table III shows the results obtained through the differential equation procedure [10]. This method was developed by Sternheimer [28] for the quadrupole polarization and antishielding effects associated with electric field gradients at nuclei, required for study of nuclear quadrupole interaction. It was applied subsequently [28] to magnetic hyperfine effects, for electron-nuclear dipolar hyperfine interactions and later to contact hyperfine interactions [29,30]. One of the latter two approaches [29] involved perturbation of the core electron states by the valence electrons in atoms by their mutual exchange interactions. The other approach [30] involved perturbation of the core electrons by the nuclear moment through the Fermi contact interaction. This latter approach, referred to as the moment perturbation method, was also applied to study ECP effects in solid state systems [31]. It was further developed [32] later to apply to the evaluation of the diagrams of many-body perturbation theory. In this method [10,32], referred to as the DE method, for each of the perturbation terms corresponding to a particular physical effect, an inhomogeneous differential equation is developed as a substitute for the infinite summation over the excited states in the perturbation expansion in Eq. (9). For example, the ECP effect of the hyperfine interaction as represented by Fig. 2(a) corresponds to the (0,1) term of the perturbation expansion and is expressed in RLCMBPT as

$$A_J(ECP) = \frac{1}{IJ}\sum_{c}^{\text{core}} \sum_{k}^{\text{exc.}(\infty)} \frac{\langle c(1)v(2)|1/r_{12}|v(1)k(2)\rangle\langle k|H'_{\text{hyp}}|c\rangle}{\varepsilon_c - \varepsilon_k} \tag{19}$$

in which c, v, and k denote the wave functions of the core, valence, and excited states, respectively, and ε_c and ε_k correspond to the energy level of the core and excited states. The DE method defines a function

$$\psi_c^{(1)} = \sum_{k}^{\text{exc.}(\infty)} \frac{\langle v(1)k(2)|1/r_{12}|c(1)v(2)\rangle|k\rangle}{\varepsilon_c - \varepsilon_k} \tag{20}$$

so now the ECP contribution to the hyperfine interaction can be expressed in a simple matrix element term

$$A_J(ECP) = \frac{1}{IJ}\sum_{c}^{\text{core}} \langle \psi_c^{(1)}|H'_{\text{hyp}}|c\rangle. \tag{21}$$

Instead of obtaining $\psi_c^{(1)}$ by summing over excited states, one obtains it in the DE method by solving the differential equation of the form

$$\begin{aligned}(\varepsilon_c - h_0)\psi_c^{(1)}(\mathbf{r}_1) = \phi_v(\mathbf{r}_1)\int \phi_v^*(\mathbf{r}_2)\frac{1}{r_{12}}\phi_c(\mathbf{r}_2)d\mathbf{r}_2 \\ -\sum_{k}^{\text{core}} \int \phi_c^*(\mathbf{r}_1)\phi_v^*(\mathbf{r}_2)\frac{1}{r_{12}}\phi_v(\mathbf{r}_1) \\ \times \phi_k(\mathbf{r}_2)d\mathbf{r}_1 d\mathbf{r}_2 \cdot \phi_k(\mathbf{r}_1),\end{aligned} \tag{22}$$

where h_0 is the Hartree-Fock Hamiltonian.

Alternately, one can evaluate the ECP diagram 2(a) by solving for the perturbation of the core electron c by the magnetic hyperfine interaction Hamiltonian H'_{hyp}, the differential equation being

$$(\varepsilon_c - h_0)\psi_c^{(2)}(\mathbf{r}_1) = H'_{\rm hyp}(\mathbf{r}_1)\phi_c(\mathbf{r}_1) - \sum_k \int \phi_k^*(\mathbf{r}_1) H'_{\rm hyp}(\mathbf{r}_1) \times \phi_c(\mathbf{r}_1) d\mathbf{r}_1 \cdot \phi_k(\mathbf{r}_1) \quad (23)$$

and then

$$A_J(ECP) = \frac{1}{IJ}\sum_c^{\rm core} \int \phi_v^*(\mathbf{r}_1)\phi_c^*(\mathbf{r}_2)\frac{1}{r_{12}}\psi_c^{(2)}(\mathbf{r}_1)\phi_v(\mathbf{r}_2)d\mathbf{r}_2 . \quad (24)$$

This second technique is more commonly used [10,11] to evaluate the ECP diagram in Fig. 2(a).

For other diagrams like the consistency diagram in Fig. 3(b), for the DE method one would have to solve appropriate differential equations for the electron-electron interaction vertex involving perturbation of a single electron. For the correlation diagram in Fig. 4(a), one needs to solve corresponding differential equations for the correlation vertex involving perturbation of two electrons. The latter equations are difficult to solve because of the simultaneous perturbation of two electrons. It is therefore difficult to evaluate higher-order correlation effects using the DE procedure.

The results in the third row of Table III give the direct and ECP contributions by the DE procedure [10]. The zeroth-order Dirac-Hartree-Fock contributions in this procedure were calculated using the $7p_{1/2}$ and $7p_{3/2}$ states as an empty excited state for the Ra^{2+} ion and this accounts for the difference seen from Table III among the values of the zeroth-order contributions by the DE procedure and those by our RLCMBPT method and the MB-MCDF approach, where in the latter two cases one uses Hartree-Fock wave functions for the $7p_{1/2}$ and $7p_{3/2}$ states of the Ra^+ ion. The smaller value for the DE calculations can be understood, as explained in our earlier RLCMBPT investigation [33] regarding the $7S_{1/2}$ state, by the fact that in the Ra^{2+} ion with the valence electron absent, the core states are more tightly bound than in the Ra^+ ion and therefore shield the nuclear charge more strongly, making the $7p_{1/2}$ and $7p_{3/2}$ states more loosely bound and therefore have a smaller density at the nucleus. The ECP result by the DE procedure is larger than our RLCMBPT result in the $7p_{3/2}$ and smaller in the $7p_{1/2}$ case. The results are closer to those obtained by the MB-MCDF approach. It is difficult to ascribe a definitive reason for this feature, since the DE procedure is not as transparent as the summation over excited states in our RLCMBPT calculations. Additionally, the use of Ra^{2+} wave functions in the DE procedure makes a quantitative comparison with our results and the MB-MCDF results difficult.

The results reported on the fourth row in Table III are obtained [11] using a combination of the DE method [10,32] and the RLCMBPT procedure for summations over excited states. Thus, for the hyperfine interaction vertex, the authors use the DE procedure to obtain the perturbation associated with the vertex while for electron-electron interaction vertices they use the summation over excited states as in the present RLCMBPT investigations. For the wave functions of the valence and excited states, they have adopted the Hamiltonians for the Ra^{2+} case. Because of this reason and the fact they have used the DE procedure for the hyperfine vertex, their results for the (0,0) and ECP contributions are close to those in Ref. [10]. The correlation contribution in Ref. [11] for the $7P_{3/2}$ case is quite close to that by the MB-MCDF procedure while in the case of the $7P_{1/2}$ state their result is substantially larger than both our RLCMBPT result and that by the MB-MCDF procedure. In view of the fact that the calculations in Ref. [11] use the Ra^{2+} wave functions and the correlation results for the $7P_{1/2}$ and $7P_{3/2}$ states compare differently with those by the MB-MCDF procedure, and also the fact that the correlation and consistency contributions do not include the role of the d shells in the MB-MCDF case, it is difficult to make conclusions about any similarities expected in the results by the two approaches, because of the fact that the DE techniques are employed although only partially in the case of Ref. [11]. It is interesting, however, to notice that as in the case of the MB-MCDF procedure, even though the individual contributions are somewhat different in detail from our RLCMBPT results, the net hyperfine constants calculated by this approach are quite close to our RLCMBPT results, which are in excellent agreement with experiment.

V. CONCLUSION

The RLCMBPT treatment of the hyperfine interactions has been successfully used here for the excited $7^2P_{3/2}$ and $7^2P_{1/2}$ states of the $^{221}Ra^+$ system. From the discussion in Sec. IV, the MB-MCDF approach [9] is an interesting alternative to the RLCMBPT method in the calculation of hyperfine properties of the atomic systems. The advantage of the RLCMBPT perturbation approach is that once the complete set of one-electron ground- and excited-state wave functions and energies are obtained, one can use them to calculate any properties including the magnetic hyperfine interaction and nuclear quadrupole interactions for an atomic system. By using the diagrammatic technique, all the physical effects contributing to these properties can be clearly illustrated and conveniently treated as perturbations to the zero-order many-particle wave function of the system. This enables one to get not only the total value of the property involved but also the breakdown of contributions from different mechanisms and therefore the physical underlining of these effects can be better understood. The RLCMBPT method requires the system to have a single determinantal configuration as in the case of a single valence electron outside closed shells, or a dominant wave function configuration as in the case of half-filled open shell. The MCDF method, on the other hand, can deal with systems with any configuration. However, because this approach uses optimization of the total energy of the system including the contribution from the property under consideration, it requires a different accurate description of the total wave function for the system for each particular property. The number of differential equations resulting from this approach can become quite large and the results obtained cannot be categorized according to the physical mechanisms as detailed in the case of the RLCMBPT method. The MB-MCDF procedure [9] incorporates some of the advantages of

both approaches. Currently, the hyperfine structures of the ground $7S_{1/2}$ and the excited $7\ ^2P_{3/2}$ and $7\ ^2P_{1/2}$ states of the $^{221}Ra^+$ ion are the only cases where this method has been applied. Further studies concerning the hyperfine interactions and other properties in different atomic systems are needed to better understand the relationship between the MB-MCDF results and the contributions from different physical effects described by the RLCMBPT approach.

[1] See, for instance, T. P. Das, Hyperfine Interactions **34**, 149 (1987), and references therein; J. Andriessen, *Many-Body Techniques in Relativistic Formulation* (Delft University Press, Delft, The Netherlands, 1980).

[2] Xing Yuan, S. N. Panigrahy, R. W. Dougherty, T. P. Das, and J. Andriessen, Phys. Rev. A **52**, 197 (1995).

[3] Mina Vajed-Samii, J. Andriessen, B. P. Das, S. N. Ray, Taesul Lee, and T. P. Das, J. Phys. B **15**, L379 (1982); A. Owusu, Ph.D. thesis, State University of New York at Albany.

[4] S. Ahmad, J. Andriessen, and T. P. Das, Phys. Rev. A **27**, 2790 (1983); S. Ahmad, J. Andriessen, K. Raghunathan, and T. P. Das, *ibid.* **25**, 2923 (1982).

[5] R. W. Dougherty, Surya N. Panigrahy, T. P. Das, and J. Andriessen, Phys. Rev. A **47**, 2710 (1993).

[6] Surya N. Panigrahy, R. W. Dougherty, T. P. Das, and J. Andriessen, Phys. Rev. A **44**, 121 (1991).

[7] S. A. Ahmad, W. Klempt, R. Neugart, E. W. Otten, K. Wendt, and C. Eckstrom, Phys. Lett. **133B**, 47 (1983); W. Neu, R. Neugart, E. W. Otten, G. Passler, K. Wendt, B. Fricke, E. Arnold, H. J. Kluge, and G. Ulm, Z. Phys. D **11**, 105 (1989).

[8] J. D. Lyons, R. T. Pu, and T. P. Das, Phys. Rev. **178**, 103 (1969); S. N. Ray, T. Lee, and T. P. Das, Phys. Rev. A **7**, 1469 (1973).

[9] J. Andriessen, H. Postma, A. M. van den Brink, and T. P. Das, Phys. Rev. A **45**, 1389 (1992).

[10] J. L. Heully and A. M. Mårtensson-Pendrill, Phys. Scr. **31**, 169 (1985).

[11] V. A. Dzuba, V. V. Flambaum, and O. P. Sushkov, Phys. Scr. **32**, 507 (1985).

[12] J. Andriessen, K. Raghunathan, S. N. Ray, and T. P. Das, Phys. Rev. B **15**, 2533 (1977); Mina Vajed-Samii, J. Andriessen, S. N. Ray, and T. P. Das, Phys. Rev. A **20**, 1787 (1979).

[13] I. P. Grant, Proc. R. Soc. London Ser. A **262**, 555 (1961).

[14] M. A. Coulthard, Proc. Phys. Soc. **91**, 44 (1967).

[15] J. P. Desclaux, D. F. Mayers, and F. O'Brien, J. Phys. B **4**, 631 (1971).

[16] T. P. Das, *Relativistic Quantum Mechanics of Electrons* (Harper & Row, New York, 1973).

[17] H. A. Bethe and E. E. Salpeter, *Quantum Mechanics of One- and Two-Electron Systems* (Springer, Berlin, 1957).

[18] H. P. Kelly, Phys. Rev. **131**, 684 (1963); **144**, 39 (1966).

[19] Edward S. Chang, Robert T. Pu, and T. P. Das, Phys. Rev. **174**, 1 (1968).

[20] James E. Rodgers, Ribha Roy, and T. P. Das, Phys. Rev. A **14**, 543 (1976).

[21] Mina Vajed-Samii, J. Andriessen, B. P. Das, S. N. Ray, T. Lee, and T. P. Das, Phys. Rev. Lett. **48**, 133 (1982); **49**, 1466 (1982); **49**, 1800 (1982); V. A. Dzuba, V. V. Flambaum, and O. P. Sushkov, J. Phys. B **17**, 1953 (1984).

[22] H. A. Bethe and J. Ashkin, *Experimental Nuclear Physics*, edited by E. Segré (Wiley, New York, 1953).

[23] K. A. Brueckner, Phys. Rev. **100**, 36 (1956); J. Goldstone, Proc. R. Soc. London Ser. A **239**, 267 (1957).

[24] Pramila Raghavan, *Table of Nuclear Moments*, At. Data Nucl. Data Tables **42** (1989).

[25] N. C. Dutta, C. Matsubara, R. T. Pu, and T. P. Das, Phys. Rev. **177**, 33 (1969).

[26] C. Froese Fisher, *The Hartree-Fock Method for Atoms* (Wiley, New York, 1977).

[27] J. Andriessen (unpublished).

[28] R. M. Sternheimer, Phys. Rev. **86**, 316 (1952); Z. Naturforsch. **41a**, 24 (1986).

[29] M. H. Cohen, D. A. Goodings, and V. Heine, Proc. Phys. Soc. London **73**, 811 (1959).

[30] G. D. Gaspari, Wei-Mei Shyu, and T. P. Das, Phys. Rev. **134**, A960 (1964); Wei-Mei Shyu, G. D. Gaspari, S. D. Mahanti, L. Tterlikkis, and T. P. Das, in *Magnetic Resonance*, edited by C. K. Coogan, N. S. Ham, S. N. Stuart, J. R. Pilbrow, and G. V. H. Wilson (Plenum, New York, 1970).

[31] Wei-Mei Shyu, G. D. Gaspari, and T. P. Das, Phys. Rev. **141**, 603 (1966); P. Jena, S. D. Mahanti, and T. P. Das, Phys. Rev. Lett. **20**, 544 (1968); S. D. Mahanti and T. P. Das, Phys. Rev. B **3**, 1599 (1971); **4**, 46 (1971); D. Ikenberry, B. K. Rao, S. D. Mahanti, and T. P. Das, J. Magn. Reson. **1**, 221 (1969).

[32] S. Garpman, I. Lindgren, and J. Morrison, Z. Phys. A **276**, 167 (1976).